Magnetic Resonance in Medicine 68:1924–1931 (2012)

Early Detection of Lung Inflammation: Exploiting T_1-Effects of Iron Oxide Particles Using UTE MRI

Klaus Strobel,[1] Verena Hoerr,[1] Florian Schmid,[1] Lydia Wachsmuth,[1] Bettina Löffler,[2] and Cornelius Faber[1]*

At high magnetic fields diagnostic proton MRI of the lung is problematic, because of fast T_2^* relaxation. The application of superparamagnetic contrast agents and the exploitation of the corresponding T_2^* effect is inefficient with conventional MRI methods, which limits the early detection of lung diseases. However, a simple theoretical treatment shows that in the lung, by the use of ultra-short echo time sequences, T_2^* effects can be neglected while T_1 shortening effects can be used for signal detection. In our study, we have applied a theoretically and experimentally optimized 3D ultra-short echo time sequence to lung phantoms and to a mouse model of lung inflammation, which was induced by systemic bacterial infection. Following the systemic application of very small superparamagnetic iron oxide nanoparticles, a significant signal increase in the lung of infected animals was detected already at 24 h postinfection, compared to control mice (17%, $P < 0.001$). Iron accumulation in the lung parenchyma as consequence of the host immune response was histologically confirmed. By conventional T_2^*- and T_2-weighted imaging, neither structural changes nor formation of substantial edema were observed. Magn Reson Med 68:1924–1931, 2012. © 2012 Wiley Periodicals, Inc.

Key words: ultra-short echo time (UTE); positive contrast; mouse lung; contrast mechanism; *Staphylococcus aureus*; bacterial infection

Proton MRI of the lung has often been considered as problematic, because large susceptibility gradients at air-tissue interfaces are abundant and give rise to very fast T_2^* relaxation at high magnetic fields. The general notion is that MRI diagnosis of lung inflammation is limited to stages with beginning edema, which locally reduces susceptibility gradients. The resulting signal can be detected with T_2-weighted or T_2^*-weighted sequences (1–4). Recently, in vivo ^{19}F detection of early infiltrating monocytes and macrophages in the lung parenchyma was reported (5). The systemic application of perfluorocarbons, which were taken up by the immune cells allowed for early detection of lung inflammation, before edema formation was observed by proton MRI. In other organs with larger T_2^* values, inflammation has been detected by proton MRI after monocytes or other immune cells had been labeled with superparamagnetic iron oxide nanoparticles (SPIOs). Cell tracking has either been performed after labeling immune cells in vitro and regrafting them (6–9), or by systemic intravenous application of SPIOs, which were then phagocytized by macrophages (10–13). T_2^* weighted sequences, such as gradient echo (GE) methods, are commonly used to subsequently detect iron labeled cells at the inflammation site. Recently, sequences providing positive contrast from iron labels have been proposed to facilitate assignment of the cellular signal (14–22). In the lung, SPIOs are regarded as useless, because strong susceptibility effects between lung parenchyma and alveolar spaces render their T_2^* effect negligible. However, if the effect of T_2^* relaxation is minimized by the use of ultra-short echo time (UTE) imaging methods, T_1-effects may become detectable and can be exploited to detect iron loaded immune cells in inflamed lungs. UTE methods (23,24) have recently gained considerable attention, culminating in an entire session at the 2011 annual meeting of the ISMRM dedicated to this topic. UTE has been shown to be able to visualize lung tissue, and different approaches have been proposed to generate positive contrast with UTE (25–28). One particularly promising approach, dubbed SubUTE, uses a double echo technique, subtracting signal acquired at normal TE from signal acquired at ultra-short TE, and thus generates positive contrast from components with fast longitudinal relaxation (28).

Here, we explore the feasibility of T_1-weighted UTE (T_1w-UTE) to detect signal increase in lung phantoms using SPIOs. With optimized parameters, the method is applicable to investigate the lung and to detect inflammation in a mouse model of bacterial lung inflammation, before substantial edema formation occurred.

THEORETICAL BACKGROUND

In molecular and cellular MRI, targets are often labeled with SPIOs (for reasons of brevity we will use the term SPIOs for all iron oxide particles in the general treatment), since these have a strong effect on T_2^* and give rise to pronounced changes in image contrast. However, if the native T_2^* of the tissue of interest is very short, the observable effect becomes small, and SPIOs less efficient. On the other hand, T_1-shortening contrast agents are most efficient in tissue with long T_1. A detailed theoretical

[1]Department of Clinical Radiology, University Hospital Muenster, Muenster, Germany.

[2]Institute of Medical Microbiology, University Hospital Muenster, Muenster, Germany.

Grant sponsor: Seventh Framework Program of the European Union; Grant number: 201842 (European Network for Cell Imaging and Tracking Expertise (ENCITE)), Grant sponsor: IZKF Muenster (core unit SAMRI), Grant sponsor: German Research Foundation: SFB 656 (project Z2), SFB TR34 (project Z3).

*Correspondence to: Cornelius Faber, Ph.D., Department of Clinical Radiology, University Hospital Muenster, Albert-Schweitzer-Campus 1, 48149 Muenster, Germany. E-mail: faberc@uni-muenster.de

Received 5 October 2011; revised 21 December 2011; accepted 4 January 2012.

DOI 10.1002/mrm.24180

Published online 24 February 2012 in Wiley Online Library (wileyonlinelibrary.com).

treatment and analysis of signal changes in UTE experiments, which are caused by the presence of contrast agents, was recently presented by Girard et al. (28). Here, we follow their considerations and apply the theory to MRI of the lung. The treatment is valid for radio frequency-spoiled sequences, with either GE or FID detection, when the pulse duration is negligible compared to T_2^* (29), the repetition time (TR) $\geq T_2^*$, and the echo time (TE) $<< T_2^*$. Further, it is assumed that in first approximation effects of field inhomogeneity, susceptibility, and chemical shift can be neglected. Under these assumptions, using the flip angle α, TR, and TE, the signal S obtained in an MR measurement can be written:

$$S = S_0 \sin(\alpha) \frac{1 - E_1}{1 - E_1 \cos(\alpha)} \exp\left(-\frac{TE}{T_2^*}\right), \quad [1]$$

with $E_1 = \exp(-TR/T_1)$. S_0 accounts for the maximum available signal given by the proton density and experimental parameters.

We assume two arbitrary tissue regions that differ in relaxation times by ΔT_1 and ΔT_2^*, but have constant relaxation times within each region T_{10} and $T_{10} - \Delta T_1$, and T_{20}^* and $T_{20}^* - \Delta T_2^*$, respectively. With these assumptions, we define the parameter $\beta = (\Delta T_2^*/T_2^*)/(\Delta T_1/T_1)$, indicating which contrast mechanism is more efficient (30). For $\beta < 1$, T_1 variations are larger than T_2^* variations, while for $\beta > 1$, T_2^* effects dominate. If the changes in relaxation times ΔT_1 and ΔT_2^* originate from a contrast agent with relaxivities r_1 and r_2^* at an iron concentration c_{Fe}, $1/T_1$ can be expressed by the usual linear approximations:

$$\frac{1}{T_1} = \frac{1}{T_{10}} + c_{\mathrm{Fe}} r_1 \quad \text{and} \quad \frac{1}{T_2^*} = \frac{1}{T_{20}^*} + c_{\mathrm{Fe}} r_2^*, \quad [2]$$

which mathematically is an expansion into a Taylor series and strictly valid only for $c_{\mathrm{Fe}} << 1$. This condition is fulfilled under most experimental situations and allows for the expression of β as (28):

$$\beta = \frac{r_2^* T_{20}^* + c_{\mathrm{Fe}} r_1 r_2^* T_{10} T_{20}^*}{r_1 T_{10} + c_{\mathrm{Fe}} r_1 r_2^* T_{10} T_{20}^*}. \quad [3]$$

For SPIO-induced contrast changes, Fig. 1a shows the parameter β for lung tissue in comparison to muscle, with longer T_2^*. Despite of the low T_1 relaxivities of SPIOs at high magnetic field, T_1 variation is the dominating relaxation mechanism for relaxation times as observed in the lung ($\beta << 1$). For relaxation times as observed in other tissues, iron oxide particles give rise to dominating T_2^* variations ($\beta > 1$). Quantitative predictions, however, are difficult. The microstructure of the lung is inhomogeneous and heterogeneous contrast agent accumulation may cause deviations from the linear approximation in Eq. 2. Consequently, we consider only signal differences for discrete relaxation time values by directly plotting Eq. 1. The read-out parameter in this study is the relative signal increase S_a/S_b, of lung tissue before (S_b) and after application of contrast agent (S_a). Suitable imaging parameters can be derived from plots of this ratio obtained directly from Eq. 1. Figures 1b,c show relative signal increase as a function of TR and FA, and TR and TE, respectively. Typical relaxation times for the lung (not contrasted and contrasted) at 9.4 T have been assumed for these plots. The highest relative signal increase is predicted if both TE and TR are minimized, and a high flip angle is applied.

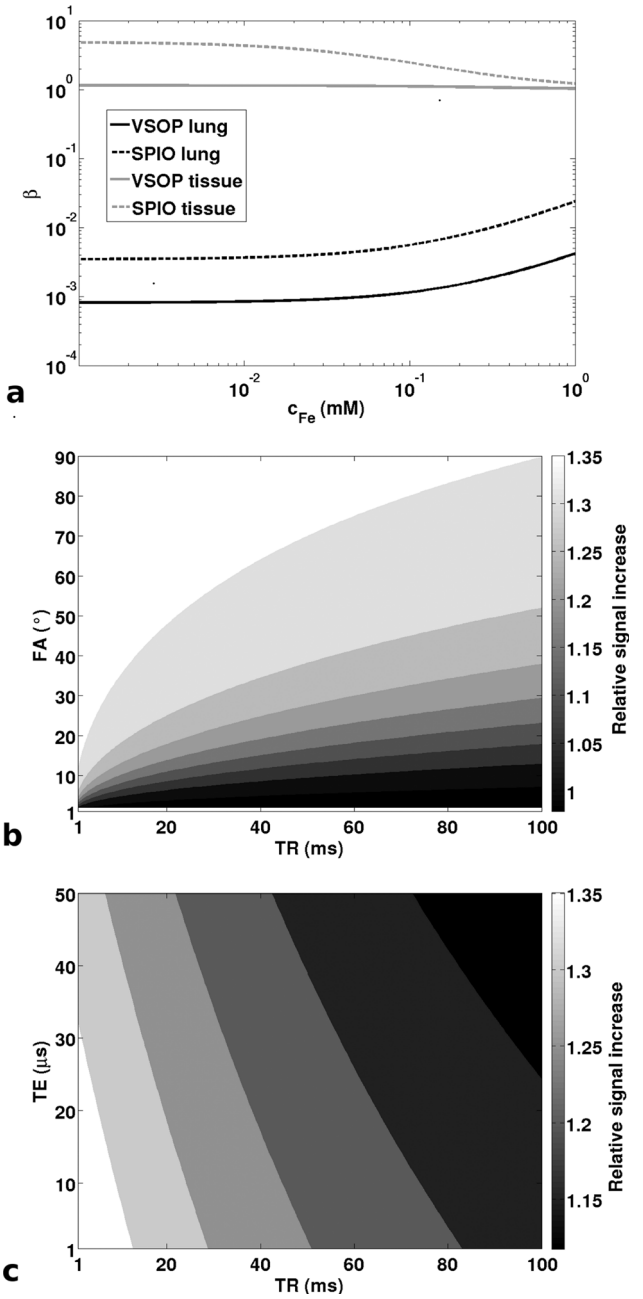

FIG. 1. Theoretical assessment of imaging parameters for optimum signal gain. **a:** Parameter β (see text) is plotted as function of the iron concentration for the lung (T_1 = 1.4 s; T_2^* = 0.1 ms, black line) and muscle [T_1 = 0.8 s; T_2^* = 80 ms, gray line (28,42)]. The solid lines represent VSOPs (r_1 = 3.2 $\mathrm{mM^{-1}\ s^{-1}}$, r_2^* = 34.3 $\mathrm{mM^{-1}\ s^{-1}}$) and the dashed lines represent SPIOs (r_1 = 4.1 $\mathrm{mM^{-1}\ s^{-1}}$, r_2^* = 210 $\mathrm{mM^{-1}\ s^{-1}}$). **b,c:** Shown is the relative signal increase (S_a/S_b, gray colorbar) according to Eq. 1 for tissue with (S_a) and without (S_b) contrast agent: T_{1a} = 1.0 s, T_{2a}^* = 0.09 ms, T_{1b} = 1.4 s, T_{2b}^* = 0.1 ms; TR-FA dependence with TE = 20 µs (b), and TR-TE dependence with FA = 50° (c).

Table 1
T_1 Relaxation Times of Lung Phantoms Containing Different Concentrations of Iron, c_{Fe}, for Homogeneously Distributed VSOPs and SPIOs

	$c_{Fe} = 0$ μM	$c_{Fe} = 0.5$ μM	$c_{Fe} = 5$ μM	$c_{Fe} = 25$ μM	$c_{Fe} = 50$ μM
VSOP[a]	2.12 ± 0.10 s[b]	2.00 ± 0.08 s[c]	1.86 ± 0.17 s[c]	1.73 ± 0.09 s[d]	1.53 ± 0.05 s[c]
SPIO[a]	2.12 ± 0.10 s[b]	2.11 ± 0.14 s[c]	1.98 ± 0.15 s[c]	1.71 ± 0.05 s[d]	1.45 ± 0.11 s[c]

[a]Experimental parameters: variable TR, TE = 20 μs, FA = 5°.
[b]Averaged over fourteen independent samples measured in 14 separate scans.
[c]Averaged over six independent samples measured in two separate scans.
[d]Averaged over three independent samples measured in one scan.

MATERIALS AND METHODS

Lung Phantoms

Hot agar gel (1% agar) was mixed with liquid soap (4% of the total volume) and stirred with a milk frother until a stable foamy texture was reached. The foam was transferred into Eppendorf tubes and subsequently cooled on ice until solidification. Bubble size ranged between 50 and 300 μm, determined by inspection with a microscope (data not shown), and thus did sufficiently well represent the alveolar geometry of tiny air-filled voids within tissue as found in the lung. To simulate iron accumulation in the lung different concentrations (0.5–50 μM iron concentration in the final volume) of 5 nm very small iron oxide nanoparticles (VSOP, C200 vivo, Ferropharm GmbH, Germany) or SPIOs (Resovist, Bayer Schering Pharma AG, Germany) were added to the agar gel of some phantoms, before the foam was produced.

Mouse Model

Animal experiments were performed with 8- to 10-week-old C57BL/6 female mice ($n = 20$) according to the guidelines of the German Regulations for Animal Welfare. The protocol was approved by the local Ethics Committee for Animal Experiments. Out of 20 animals, $n = 4$ were used as controls and sacrificed without any injection; two of them were scanned by MRI before sacrifice. The remaining 16 animals were scanned before any injection, resulting in an MRI control group of $n = 18$ mice. From the remaining 16 mice, $n = 6$ received injection of bacteria and VSOP; two groups of $n = 5$ each received injections of either bacteria or VSOP. Bacterial infection was induced by tail vein injection of 100 μL of a suspension of *Staphylococcus aureus* (1×10^8 colony forming units per mL). The bacteria cause a systemic infection, resulting in inflammation of the lung, which peaks at 6 h after injection (31). The systemic induction causes milder forms of lung inflammation than the typically used brute force methods of intratracheal instillation of bacterial suspensions or inflammatory substances (1–4). At 2 and 5 h after infection, before the expected peak of the immune response, 300 μmol Fe/kg VSOPs were injected i.v. Mice were imaged 24 h after infection. A tube containing SPIOs in water at a concentration of 50 μM was placed next to the flank of the animal. To reduce susceptibility artifacts at the air-tube interface the tube was embedded in alginate gel (32), covering the flank of the mouse. Animals were anaesthetized with 1.5% isoflurane in 1 L/min O_2/compressed air (20:80) delivered through a face mask. After the final (24 h) MRI scan all mice were sacrificed by CO_2 asphyxiation. Lungs were excised and visually examined for signs of inflammation (swelling, darker color of the lung).

MRI

Measurements were performed with a 9.4 T small animal magnetic resonance scanner with 20 cm bore size (BioSpec 94/20; Bruker BioSpin MRI GmbH, Germany) equipped with a micro imaging gradient coil system (gradient strength, 1000 mT/m) and a 35 mm quadrature birdcage coil. The system was operated using the software ParaVision 5.1. (Bruker BioSpin MRI GmbH, Germany), which provided a pulse program for 3D UTE MRI. The gradient trajectory distortion was measured in a preceding scan and was used for reconstruction of all scans with identical geometry.

MRI of Lung Phantoms

We tested four different iron concentrations. For each iron concentration, two sets of five tubes each were scanned simultaneously: one tube with pure agar gel, to provide sufficient coil loading and signal for automatic shimming and power adjustment; one tube with pure foam as a reference; and three tubes with foam, containing equal concentrations of iron oxide particles. TR, TE, and FA in the UTE sequence were chosen to maximize the signal increase in lung phantoms with SPIOs, compared to lung phantoms without contrast agent. Based on the theoretical considerations TE = 20 μs and TR = 8 ms were used. Signal intensity in a central ROI in each tube was measured with ParaVision. For each concentration we report the mean and the standard deviations from several tubes, which were measured in two separate experiments, if not indicated otherwise in Table 1.

T_1 measurements were performed with UTE at TE = 20 μs and FA = 5, 15, and 50°, and multiple TRs of 10, 25, 50, 75, 100, 200, and 500 ms. T_1 fitting with Eq. 1 was performed with MATLAB R2010a (The MathWorks).

T_2^* of the lung phantoms was estimated by acquiring the FID signal from a single tube, assuming a single exponential decay. To calculate the relaxivity r_1 of VSOPs and SPIOs, Eq. 2 was fitted to the measured T_1 relaxation times for the different iron concentrations. r_2^* relaxivities were extrapolated to 9.4 Tesla from literature values (12) [VSOPs ($r_2^* = 34.3\ mM^{-1}\ s^{-1}$); SPIOs ($r_2^* = 210\ mM^{-1}\ s^{-1}$)].

In Vivo MRI

In vivo measurements were performed with the same sequence used for the phantoms with TR = 8 ms,

TE = 20 μs, FA = 5° and 50°, measurement time = 7 min, number of projections = 51,360, block pulse excitation of 20 μs duration, field of view (FOV) = 4 × 4 × 4 cm^3, matrix = 128 × 128 × 128, resulting in a nominal spatial resolution of 310 × 310 × 310 μm^3. No triggering or gating was applied to keep the steady state of the magnetization. T_1 of the mouse lung was estimated from UTE measurements with TE = 20 μs and FA = 5° using multiple TRs of 8, 15, 25, 50, 75, and 150 ms. T_1 was calculated by fitting the data with Eq. 1.

Additionally, multislice coronal GE (FLASH, TR = 400 ms, TE = 6 ms, FA = 30°, FOV = 3 × 3 cm^2, Matrix = 256 × 256, slice thickness = 0.7 mm) and multislice coronal RARE (TR = 2500 ms, TE = 33 ms, FOV = 3 × 3 cm^2, Matrix = 256 × 256, slice thickness = 0.7 mm, RARE factor = 8) images were recorded. Acquisition of the images was triggered by the breathing mode using a small animal gating device (SA Instruments) connected to an air-pillow placed under the animal. Depth of anesthesia was controlled to keep the breathing rate constant at ~50 breath/min.

Histology

Lungs were dissected, fixed in 3.7% formalin solution, and embedded in paraffin. The stage-mounted lungs were cut with a microtome (RM2235, Leica Instruments, Germany) into 5 μm horizontal sections, which were mounted onto microscope slides. To visualize the iron content, the lung sections were stained with potassium ferrocyanide (Prussian blue).

Analysis

For all experimental data relative signal changes were calculated by dividing the average signal from comparable ROIs. To compensate for interscan variations signal intensities were divided by the mean intensity from a central ROI in the reference tube, which was present in all analyzed image slices. For the in vivo data, signal intensities in the lungs were measured in one representative coronal slice, located 10 slices (~3.1 mm) dorsal to the rim of the mouse heart. At this slice location, the contribution from intravascular signal was limited and minimal artifacts due to blood flow in the vessels were observed. The lung ROI was drawn manually in the standard UTE image (FA = 5°) and subsequently copied to the corresponding T_1w-UTE image.

Descriptive data were expressed as arithmetic means ± standard deviations. Differences were considered significant at $P < 0.05$ (Wilcoxon rank sum test).

RESULTS

Feasibility Assessment in Lung Phantoms

We have implemented a 3D UTE sequence with TE values as short as 20 μs and very small TR, which opened the possibility to experimentally exploit T_1 effects in lung tissue in vivo. The validity of the theoretical estimations was confirmed by assessing lung phantoms consisting of agar gel with foam like texture, which mimicked the alveolar structure of the lung. T_1 relaxation times of lung phantoms steadily decreased with increasing iron concentration. The T_1 shortening effect was observed in the micromolar iron concentration range (Table 1). Standard deviations were not dominated by the quality of the fit, but rather by averaging over several phantoms with slightly different texture. To show the reproducibility of T_1 measurements, one lung phantom was measured with different FAs, for VSOP concentration of 50 μM. T_1 values of 1.52 ± 0.04 s, 1.61 ± 0.07 s, and 1.59 ± 0.07 s were obtained for FAs of 5°, 15°, and 50°, respectively. From the measurement with FA = 5° the relaxivity r_1 in the lung phantoms was calculated for VSOPs (r_1 = 3.2 ± 0.8 mM^{-1} s^{-1}) and SPIOs (r_1 = 4.1 ± 0.6 mM^{-1} s^{-1}) based on a linear relation between T_1 and the iron concentration (Eq. 2). Relatively large standard deviations were attributed to differences in the distribution of pore sizes in the foam between the individual phantoms. We estimated T_2^* values between 0.05 and 0.15 ms from the FID signal. Accordingly, the GE sequence did not provide images with signal above noise level, while UTE yielded sufficient signal for further analysis.

As predicted by the theoretical considerations, the relative signal increase, S_a/S_b, between lung phantoms with (S_a) and phantoms without contrast agent (S_b), increased with higher flip angles (Fig. 2a). Due to power limitations for the extremely short pulse durations required to achieve TE = 20 μs, maximum pulse angles were limited to 60°. Assuming a T_2^* of 100 μs for the phantom with pure foam and a T_2^* of 60 μs (95 μs) for the phantom with VSOPs (SPIOs), the theoretical curve matched the experimental data within the error bars. The TR dependence of the experimental data also matched the theoretical curves (Fig. 2b). Highest signal increase was observed for the shortest TR value of 8 ms for three FAs of 5, 15, and 50°. The large difference between the FAs observed for long TR, decreased substantially for short TR. Based on these results the parameters TR = 8 ms, TE = 20 μs, and FA = 50° were chosen for the T_1w-UTE experiments. With regard to iron concentration the relative signal gain in T_1w-UTE increased with higher concentrations. It reached 18 and 49%, for VSOPs and SPIOs, respectively, as plotted for each concentration in Fig. 2c.

Detection of Lung Inflammation In Vivo

To assess whether T_1w-UTE is suitable for early detection of lung inflammation in vivo, measurements were performed in a mouse model of bacterial infection. Preliminary scans showed that in the healthy mouse lung T_1 was ~1.4 s and T_2^* below 1 ms. This observation suggested that T_1 effects of administered iron oxide particles would be detectable using T_1w-UTE. Figure 3 shows representative images of an infected mouse after administration of iron particles (a–c), and a control mouse (d–f). Lung, liver, and muscle tissue of control animals were well delineated. After application of iron particles (data not shown for animals without infection) contrast between liver and lung strongly decreased. The reference tube was visible in all images. The alginate, embedding the tube and covering the animals' chest, was clearly visible in UTE images, while alginate was not observed in the GE images. Similarly, lung parenchyma was not

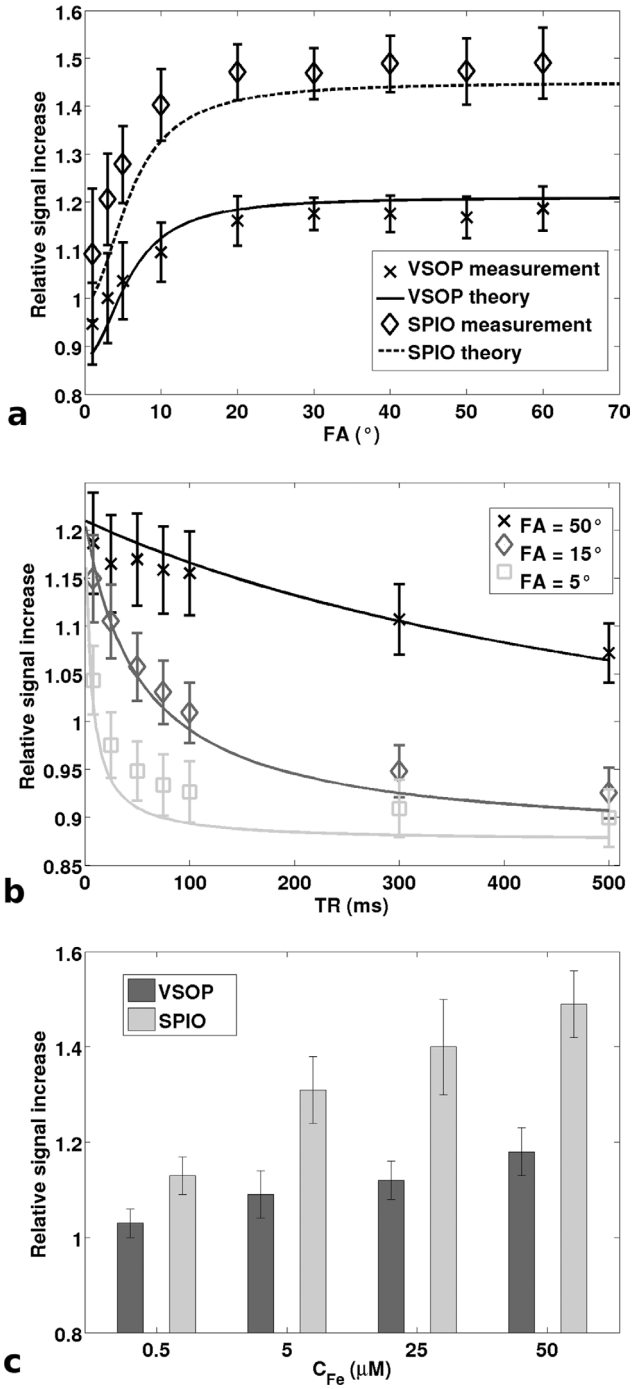

FIG. 2. Relative signal increase in 3D T_1w-UTE measurements of lung phantoms. Relative signal increase (S_a/S_b) for phantoms with (S_a) and without (S_b) contrast agent is shown in **(a)** at different FA, for both VSOPs and SPIOs, **(b)** at different TR, for VSOPs, and **(c)** at different iron concentration, for both VSOPs and SPIOs. Data points are the experimental means; standard deviations are indicated. Experimental parameters were TE = 20 μs; TR = 8 ms, FA = 60°, and c_{FE} = 50 μM, if not indicated otherwise. Solid lines in (a) and (b) show theoretical curves according to Eq. 1 for VSOPs: T_{1a} = 1.53 s, T_{2a}^* = 0.06 ms, T_{1b} = 2.12 s, T_{2b}^* = 0.1 ms. The dashed line in (a) shows the theoretical curve for SPIOs: T_{1a} = 1.45 s, T_{2a}^* = 0.095 ms, T_{1b} = 2.12 s, T_{2b}^* = 0.1 ms. T_1 values have been measured (Table 1). It is important to note that theoretical curves only show the qualitative agreement, since T_2^* values were set arbitrarily within the experimentally observed limits.

visible in GE images, while UTE images provided sufficient SNR for the further analysis.

Lung inflammation could be detected at 24 h after infection with in vivo T_1w-UTE. The signal intensities of the lung were compared between four groups, as shown in Fig. 4a: a) the control group, b) the group that had received both bacteria and VSOP, c) the group that had received only bacteria and d) the group with VSOP injection only. The infected and contrasted group showed a significant signal increase of 17% ($P < 0.001$) compared to the control group. An increase of 25% ($P < 0.01$) and 18% ($P < 0.05$) was found in comparison to the groups that had received only bacteria or VSOP, respectively. No significant differences were observed between the other three groups. In vivo measurements with different shimming conditions and at different respiration rates, ranging from 40 to 80 breath/min, showed that the signal in the healthy lung varied by less than 8% between individual scans (data not shown).

No significant signal differences were observed in the lung using standard UTE (FA = 5°), FLASH or RARE sequences (Fig. 4b). While UTE resulted in low standard deviations, the sequences with longer echo times showed substantial deviations between individual animals, emphasizing that MRI of the lung is still challenging at high magnetic fields. Our data show that T_1w-UTE provides the possibility to detect lung inflammation after systemic application of iron oxide particles only 24 h after bacterial infection. At this time point no signs of edema formation were observed in GE or T_2-weighted images. Successful application of VSOP was confirmed by pronounced contrast changes in the liver in all animals that had received VSOP, either alone or in combination with bacteria (see Fig. 3). Actual induction of an inflammatory response was confirmed by postmortem macroscopical and histological analysis of the lungs. All lungs of infected animals showed clear signs of inflammation (swelling, darker color), while lungs of controls and animals that had received only VSOP appeared normal. In none of the lungs were signs of substantial edema formation observed. Prussian blue staining of the sectioned lungs revealed strong iron accumulations only in animals which had received both, bacteria and VSOP. No such accumulation was observed in controls or animals that had received either VSOP or bacteria alone (Fig. 5).

DISCUSSION

In the present study, we have applied an UTE imaging sequence to detect T_1 changes induced by iron oxide particles in the mouse lung. The work is based on the awareness that despite the inefficiency of detecting T_2^* effects in the lung, T_1 changes induced by SPIOs become observable with T_1w-UTE. The theoretical treatment summarized in Fig. 1 explains the experimental findings, which are summarized in Figs. 2 and 4. Still, T_2^* relaxation has a strong influence on the actual signal increase. For larger T_2^* differences, the theoretical curves would be shifted to smaller signal increase (cf. Fig. 2a). Since a T_2^* of ~0.1 ms could not be measured quantitatively in this study, it must be concluded that the theoretical curves predict the data qualitatively. Further, variations

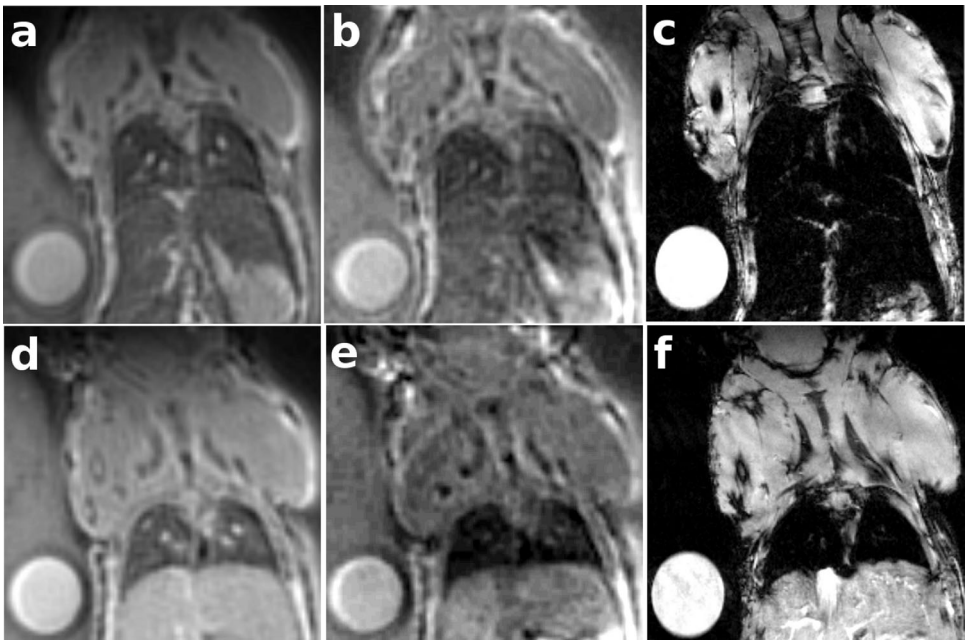

FIG. 3. In vivo MRI of the mouse lung. Representative coronal slices show mouse lungs of an infected animal (24 h postinfection) after systemic application of VSOP **(a–c)** and a control animal **(d–f)**. **a,d:** standard UTE (FA = 5°), **(b,e)** T_1w-UTE (FA = 50°), and **(c,f)** FLASH images show a prominent signal decrease in the liver signal after contrast agent application. Signal from lung parenchyma and alginate is only observed in the standard UTE and T_1w-UTE images. The reference tube containing SPIOs in water at an iron concentration of 50 μM is clearly visible in all images.

due to local iron accumulation cannot be ruled out. A strong influence of microstructural changes in the lung on relaxation mechanisms has previously been reported in other in vivo studies (1,33,34). Within these limitations, theory and experiments confirm that UTE with the chosen parameters yields T_1 weighted images. On the contrary, UTE with longer TR or smaller FA, produces spin density weighted images. T_2^* weighting can be achieved by increasing TE. Combined T_1 and T_2^* contrast can be achieved using a double echo technique with subsequent image subtraction (28). Last but not least, T_2 weighted UTE can be performed with suitable preparation pulses, as recently demonstrated by Kirsch and Schad (35).

T_1w-UTE has to be performed in 3D, or in 2D with half pulse excitation to reach the extremely short TE values that are required to exploit positive T_1 contrast. 3D UTE requires extended scan times and, consequently, limits the achievable spatial resolution, as well as the number of scans with different parameters that can be performed during a reasonable examination time in vivo. One possible strategy to reduce scan times or to increase the in-plane resolution is the application of 2D versions of UTE. Unfortunately, this is not an option for imaging of the lung. Excitation pulses of several hundred microseconds have to be applied for slice selection, which results in TE values in the same range and thus sacrifices any signal increase obtained by 3D T_1w-UTE (see Fig. 1c). An alternative method to achieve very short TE is the application of half pulses for slice-selective excitation (36,37), and subsequently adding up two consecutively acquired free induction decays with complementary gradients. This elegant method, however, is ruled out by the following reasons: Proper slice selection with half pulses relies on a homogeneous magnetic field (36,37), a condition which is not given in the lung at high magnetic fields, in particular in presence of iron accumulation. Even with motion compensation, addition of two consecutively acquired free induction decays

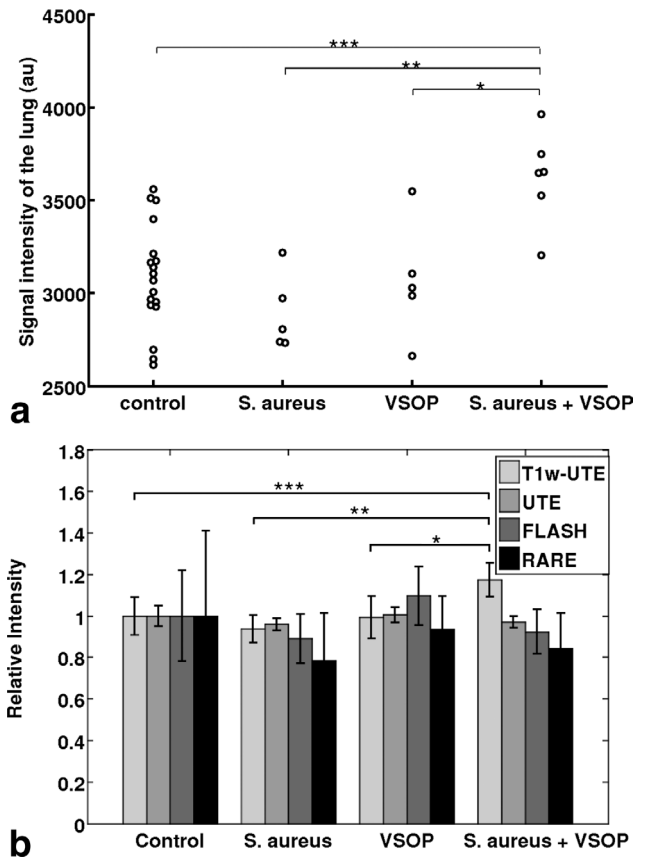

FIG. 4. Detection of lung inflammation with UTE. **a:** Scatter plot shows the signal intensities of the lung of four different groups of mice using T_1w-UTE (FA = 50°). **b:** Bar plot shows the signal intensities (including the standard deviation) of T_1w-UTE (FA = 50°), standard UTE (FA = 5°), FLASH, and RARE images of the four different groups. The image intensities were referenced to the control group that was scaled to one. Statistical significant differences are marked with asterisks (*: $P < 0.05$; **: $P < 0.01$; ***: $P < 0.001$).

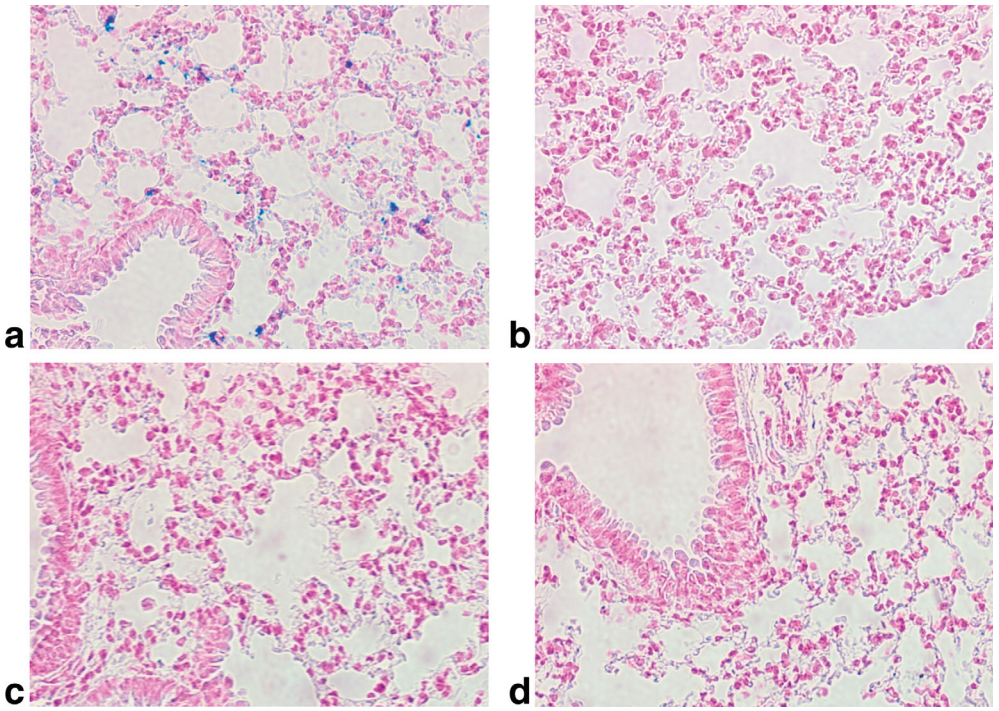

FIG. 5. Iron content in the lung. Representative histological slices (×40) show Prussian blue staining of the mouse lung. Iron accumulation appears in blue in an animal infected with *S. aureus* and subsequent VSOP injection **(a)**. Animals having received only VSOP injection **(b)**, or having received only injection of *S. aureus* **(c)**, or without any injection **(d)** show no blue staining, i.e., no iron accumulation in the lung.

would not result in meaningful slice selection. Due to the opposite sign of the applied slice selection gradients, slice profiles would not be identical. Although previous studies have reported successful 2D UTE imaging of the lung ex vivo (23) and in vivo (38), the magnetic field strength of 9.4 T, slice thickness of only 1 mm and high breathing frequency of the mouse prohibit this technique.

Our measurements have demonstrated that with T_1w-UTE, lung inflammation in a mouse model of systemic bacterial infection can be detected before edema formation. Previously, proton MRI detection of lung inflammation relied on methods with TE in the millisecond range. Only after formation of substantial edema, susceptibility effects were reduced to a level that signal from the lung became detectable (5,39). GE methods with very short TE (1) or single point imaging methods (33) are also possible, but require long scan times or provide only limited resolution. Therefore, such MR sequences are not suitable to detect mild forms of inflammation. By applying T_1w-UTE, significant signal increase in the mouse lung was obtained from iron accumulation in the lung, following the host immune response. Iron load together with the enhanced sensitivity towards T_1 effects allowed for detection of inflammation at earlier time points and also of milder forms than in previous studies (1,3,5,39–41).

CONCLUSION

In this study, we have shown that T_1 changes in response to iron oxide accumulation in the mouse lung can be detected as increased signal, if a 3D T_1w-UTE sequence is used. Based on the systemic application of iron oxide particles, T_1w-UTE allows for early detection of lung inflammation following a bacterial infection. T_1w UTE represents a sensitive positive contrast method to detect iron oxide particle accumulation at inflammation sites even in tissues with very fast transversal relaxation times, like the lung. The application to other models of mild lung inflammation and parameter optimization for clinically approved iron-containing contrast agents may pave the way to apply T_1w-UTE in patients in the future.

REFERENCES

1. Beckmann N, Tigani B, Mazzoni L, Fozard JR. MRI of lung parenchyma in rats and mice using a gradient-echo sequence. NMR Biomed 2001;14:297–306.
2. Tigani B, Schaeublin E, Sugar R, Jackson AD, Fozard JR, Beckmann N. Pulmonary inflammation monitored noninvasively by MRI in freely breathing rats. Biochem Biophys Res Commun 2002;292:216–221.
3. Marzola P, Lanzoni A, Nicolato E, Di Modugno V, Cristofori P, Osculati F, Sbarbati A. (1)H MRI of pneumococcal pneumonia in a murine model. J Magn Reson Imaging 2005;22:170–174.
4. Olsson LE, Smailagic A, Onnervik PO, Hockings PD. (1)H and hyperpolarized (3)he MR imaging of mouse with LPS-induced inflammation. J Magn Reson Imaging 2009;29:977–981.
5. Ebner B, Behm P, Jacoby C, Burghoff S, French BA, Schrader J, Flogel U. Early assessment of pulmonary inflammation by 19F MRI in vivo. Circ Cardiovasc Imaging 2010;3:202–210.
6. Wang YX, Hussain SM, Krestin GP. Superparamagnetic iron oxide contrast agents: Physicochemical characteristics and applications in MR imaging. Eur Radiol 2001;11:2319–2331.
7. Bernsen MR, Moelker AD, Wielopolski PA, van Tiel ST, Krestin GP. Labelling of mammalian cells for visualisation by MRI. Eur Radiol 2010;20:255–274.
8. von zur Muhlen C, Fink-Petri A, Salaklang J, Paul D, Neudorfer I, Berti V, Merkle A, Peter K, Bode C, von Elverfeldt D. Imaging monocytes with iron oxide nanoparticles targeted towards the monocyte integrin MAC-1 (CD11b/CD18) does not result in improved atherosclerotic plaque detection by in vivo MRI. Contrast Media Mol Imaging 2010;5:268–275.
9. Ottobrini L, Martelli C, Trabattoni DL, Clerici M, Lucignani G. In vivo imaging of immune cell trafficking in cancer. Eur J Nucl Med Mol Imaging 2011;38:949–968.
10. Dousset V, Delalande C, Ballarino L, Quesson B, Seilhan D, Coussemacq M, Thiaudiere E, Brochet B, Canioni P, Caille JM. In vivo macrophage activity imaging in the central nervous system detected by magnetic resonance. Magn Reson Med 1999;41:329–333.

11. Rausch M, Baumann D, Neubacher U, Rudin M. In-vivo visualization of phagocytotic cells in rat brains after transient ischemia by USPIO. NMR Biomed 2002;15:278–283.
12. Corot C, Port M, Guilbert I, Robert P, Raynal I, Robic C, Raynaud JS, Prigent P, Dencausse A, Idee JM. Superparamagnetic contrast agents. In: Modo MMJ, Bulte JWM, editors. Molecular and cellular MR imaging. Boca Raton: Taylor & Francis; 2007. pp59–83.
13. Hoehn M, Wiedermann D, Justicia C, Ramos-Cabrer P, Kruttwig K, Farr T, Himmelreich U. Cell tracking using magnetic resonance imaging. J Physiol 2007;584 (Part 1):25–30.
14. Seppenwoolde JH, Viergever MA, Bakker CJ. Passive tracking exploiting local signal conservation: the white marker phenomenon. Magn Reson Med 2003;50:784–790.
15. Cunningham CH, Arai T, Yang PC, McConnell MV, Pauly JM, Conolly SM. Positive contrast magnetic resonance imaging of cells labeled with magnetic nanoparticles. Magn Reson Med 2005;53:999–1005.
16. Mani V, Briley-Saebo KC, Itskovich VV, Samber DD, Fayad ZA. Gradient echo acquisition for superparamagnetic particles with positive contrast (GRASP): sequence characterization in membrane and glass superparamagnetic iron oxide phantoms at 1.5T and 3T. Magn Reson Med 2006;55:126–135.
17. Zurkiya O, Hu X. Off-resonance saturation as a means of generating contrast with superparamagnetic nanoparticles. Magn Reson Med 2006;56:726–732.
18. Dharmakumar R, Koktzoglou I, Li D. Generating positive contrast from off-resonant spins with steady-state free precession magnetic resonance imaging: theory and proof-of-principle experiments. Phys Med Biol 2006;51:4201–4215.
19. Faber C, Heil C, Zahneisen B, Balla DZ, Bowtell R. Sensitivity to local dipole fields in the CRAZED experiment: an approach to bright spot MRI. J Magn Reson 2006;182:315–324.
20. Stuber M, Gilson WD, Schar M, Kedziorek DA, Hofmann LV, Shah S, Vonken EJ, Bulte JW, Kraitchman DL. Positive contrast visualization of iron oxide-labeled stem cells using inversion-recovery with ON-resonant water suppression (IRON). Magn Reson Med 2007;58:1072–1077.
21. Liu W, Dahnke H, Jordan EK, Schaeffter T, Frank JA. In vivo MRI using positive-contrast techniques in detection of cells labeled with superparamagnetic iron oxide nanoparticles. NMR Biomed 2008;21: 242–250.
22. Patil S, Jirak D, Saudek F, Hajek M, Scheffler K. Positive contrast visualization of SPIO-labeled pancreatic islets using echo-dephased steady-state free precession. Eur Radiol 2011;21:214–220.
23. Bergin CJ, Pauly JM, Macovski A. Lung parenchyma: projection reconstruction MR imaging. Radiology 1991;179:777–781.
24. Robson MD, Gatehouse PD, Bydder M, Bydder GM. Magnetic resonance: An introduction to ultrashort TE (UTE) imaging. J Comput Assist Tomogr 2003;27:825–846.
25. Rahmer J, Blume U, Bornert P. Selective 3D ultrashort TE imaging: comparison of "dual-echo" acquisition and magnetization preparation for improving short-T 2 contrast. Magn Reson Mater Phys 2007;20:83–92.
26. Coolen BF, Lee P, Shuter B, Golay X. Optimized MRI Parameter for Positive Contrast Detection of Iron-Oxide Labeled Cells Using Double-Echo Ultra-Short Echo Time (D-UTE) Sequences. In: Proceedings of the 15th Annual Meeting of ISMRM, Berlin, Germany, 2007. p 262.
27. Diwoky C, Reinisch A, Gross D, Lehmann V, Strunk D, Stollberger R. UTE Imaging for Single Cell Detection with Positive Contrast. In: Proceedings of the 17th Annual Meeting of ISMRM, Honolulu, Hawaii, USA, 2009. p 805.
28. Girard OM, Du J, Agemy L, Sugahara KN, Kotamraju VR, Ruoslahti E, Bydder GM, Mattrey RF. Optimization of iron oxide nanoparticle detection using ultrashort echo time pulse sequences: comparison of T(1), T(2) *, and synergistic T(1) – T(2) * contrast mechanisms. Magn Reson Med 2011;65:1649–1660.
29. Carl M, Bydder M, Du J, Takahashi A, Han E. Optimization of RF excitation to maximize signal and T2 contrast of tissues with rapid transverse relaxation. Magn Reson Med 2010;64:481–490.
30. Buxton RB, Edelman RR, Rosen BR, Wismer GL, Brady TJ. Contrast in rapid MR imaging: T1- and T2-weighted imaging. J Comput Assist Tomogr 1987;11:7–16.
31. Yi C, Cao Y, Mao SH, Liu H, Ji LL, Xu SY, Zhang M, Huang Y. Recombinant human growth hormone improves survival and protects against acute lung injury in murine staphylococcus aureus sepsis. Inflamm Res 2009;58:855–862.
32. Strobel K, Bergmann R, Meister S, van den Hoff J, Pietzsch J. Improved multimodality imaging using alginate molding in xenograft tumor models. J Magn Reson Imaging 2010;31:747–752.
33. Olsson LE, Lindahl M, Onnervik PO, Johansson LB, Palmer M, Reimer MK, Hultin L, Hockings PD. Measurement of MR signal and T_2^* in lung to characterize a tight skin mouse model of emphysema using single-point imaging. J Magn Reson Imaging 2007;25:488–494.
34. Takahashi M, Togao O, Obara M, van Cauteren M, Ohno Y, Doi S, Kuro-O M, Malloy C, Hsia CC, Dimitrov I. Ultra-short echo time (UTE) MR imaging of the lung: comparison between normal and emphysematous lungs in mutant mice. J Magn Reson Imaging 2010; 32:326–333.
35. Kirsch S, Schad LR. Single-slice mapping of ultrashort T(2). J Magn Reson 2011;210:133–136.
36. Nielsen HT, Gold GE, Olcott EW, Pauly JM, Nishimura DG. Ultrashort echo-time 2D time-of-flight MR angiography using a half-pulse excitation. Magn Reson Med 1999;41:591–599.
37. Robson MD, Gatehouse PD. Consequences of T2 relaxation during half-pulse slice selection for ultrashort TE imaging. Magn Reson Med 2010;64:610–615.
38. Kauczor HU, Kreitner KF. MRI of the pulmonary parenchyma. Eur Radiol 1999;9:1755–1764.
39. Conti G, Tambalo S, Villetti G, Catinella S, Carnini C, Bassani F, Sonato N, Sbarbati A, Marzola P. Evaluation of lung inflammation induced by intratracheal administration of LPS in mice: comparison between MRI and histology. Magn Reson Mater Phys 2010;23:93–101.
40. Beckmann N, Cannet C, Karmouty-Quintana H, Tigani B, Zurbruegg S, Ble FX, Cremillieux Y, Trifilieff A. Lung MRI for experimental drug research. Eur J Radiol 2007;64:381–396.
41. Ripoll J, Ntziachristos V, Cannet C, Babin AL, Kneuer R, Gremlich HU, Beckmann N. Investigating pharmacology in vivo using magnetic resonance and optical imaging. Drugs R D 2008;9:277–306.
42. Tadamura E, Hatabu H, Li W, Prasad PV, Edelman RR. Effect of oxygen inhalation on relaxation times in various tissues. J Magn Reson Imaging 1997;7:220–225.